Composite Tube Hinges

J. C. H. Yee[1] and S. Pellegrino[2]

Abstract: This paper is concerned with self-powered, self-latching tube hinges, made by cutting three parallel slots in a thin-walled carbon fiber reinforced plastic tube with a circular cross section. Thus, a hinge consists of two short tubes connected by three transversally curved strips of material (known as tape springs). A particular tube hinge design is considered, with a diameter of about one-third that of the hinges used previously; this requires the tape springs to reach strains close to failure when the hinge is folded. Three analyses of the peak strains in a tube hinge are presented. The first analysis obtains general analytical expressions for the longitudinal fold radius of a tape spring and the associated peak fiber strains. The second analysis is a finite-element simulation of the folding of a single tape spring and the third analysis is a simulation of a complete tube hinge. It is found that the largest fiber strains in one- and two-ply hinges can be predicted analytically with very good accuracy. It is also found that the contact and interaction between the three tape springs that form a tube hinge, modeled in the third analysis, do not affect the peak strains significantly.

DOI: 10.1061/(ASCE)0893-1321(2005)18:4(224)

CE Database subject headings: Tubes; Hinges; Composite materials; Thin shell structures; Fiber reinforced plastics.

Introduction and Background

There is a growing trend in the aerospace industry toward simpler, cheaper, and more reliable deployable structures. Research is being carried out into new structural concepts that can provide enhanced levels of functionality in comparison with current designs for deployable booms, solar arrays, etc., while also requiring a smaller number of separate parts. One approach that is currently being pursued is the development of new structural components which can be manufactured through shorter and simpler processes, and in which several different functions are combined.

This new approach has produced the self-powered, self-latching tube hinge shown in Fig. 1, which is a replacement for a traditional spring-driven pin-and-clevis hinge fitted with a latch. Unlike a traditional mechanical hinge, the tube hinge does not require any lubrication. The tube hinge considered in this paper is made by cutting three parallel slots in a thin-walled carbon fiber reinforced plastic (CFRP) tube with a circular cross section. The slots divide the tube into three strips that are transversally curved; these strips—known as tape springs—can be flattened transversally and then bent longitudinally to form a localized fold in the middle of the tube hinge, as shown in Fig. 1.

Tube hinges are designed such that their deformation during folding is entirely elastic. Because the ends of the tube remain essentially undeformed, only the deformation of the tape springs needs to be analyzed. More precisely, the folding of a tube hinge can be described in terms of the tape spring on the inside of the fold deforming in *opposite-sense bending* and the two outer tape springs deforming in *equal-sense bending*. Here equal-sense bending indicates that the bent tape spring has the same convexity as the straight one, see Fig. 2(a); in this case the edges of the tape spring are under *compression*. Conversely, opposite-sense bending indicates that the bent tape spring has opposite convexity to the straight one, Fig. 2(b), in which case the edges of the tape spring are under *tension*. Tape springs made of isotropic materials (typically beryllium–copper or steel) have been used for many years, and their behavior is well understood (Rimrott 1970; Calladine 1988; Seffen and Pellegrino 1999).

When an initially straight tape spring is subject to gradually increasing equal and opposite end rotations, at first it takes a uniform, longitudinally curved shape. For sufficiently small rotations its moment–rotation relationship is linear; for larger rotations the relationship becomes nonlinear, as follows. For opposite-sense bending, when the end rotations reach a critical value the tape spring suddenly snaps and forms an elastic fold that is approximately straight in the transverse direction and has approximately uniform longitudinal curvature, see Fig. 2(b). Then, if the rotations are further increased, the arc length of the fold increases whereas its curvature remains constant. For equal-sense bending the tape spring deforms by gradually twisting over two adjacent, but separate, regions whose lengths grow until the two folds merge into a single, localized fold. Once this single fold has formed, Fig. 2(a), further increasing the end rotations results—

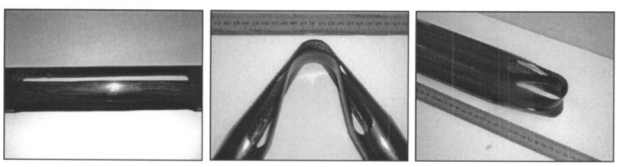

Fig. 1. Carbon fiber reinforced plastic tube hinge (unfolded, folded 110°, and folded 180°)

[1]Dept. of Engineering, Univ. of Cambridge, Trumpington St., Cambridge CB2 1PZ, U.K.

[2]Dept. of Engineering, Univ. of Cambridge, Trumpington St., Cambridge CB2 1PZ, U.K. (corresponding author). E-mail: pellegrino@eng.cam.ac.uk

Note. Discussion open until March 1, 2006. Separate discussions must be submitted for individual papers. To extend the closing date by one month, a written request must be filed with the ASCE Managing Editor. The manuscript for this paper was submitted for review and possible publication on September 15, 2003; approved on August 31, 2004. This paper is part of the ***Journal of Aerospace Engineering***, Vol. 18, No. 4, October 1, 2005. ©ASCE, ISSN 0893-1321/2005/4-224–231/$25.00.

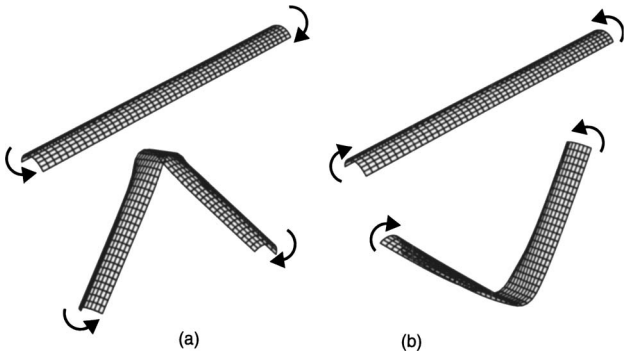

Fig. 2. Two different ways of folding a tape spring: (a) equal-sense bending; and (b) opposite-sense bending

again—only in an increase of the arc length of the fold region. When it is released, a folded tape spring has a natural tendency to deploy, thus resuming its straight configuration.

A tube hinge contains three tape springs, and hence the deployment moment of a complete hinge is significantly higher than that of a single tape spring. Also the moment that the hinge can resist without starting to fold is much higher.

This paper considers a particular tube hinge design, with a diameter of about one-third that of the hinge shown in Fig. 1. This design requires the tape springs to fold so tightly that they come into contact, and have to operate close to failure. Hence, a detailed analysis of the strains induced by the folding process is required. In fact, three analyses of increasing complexity and sophistication will be carried out, of which the first is based on an extension to orthotropic materials of Rimrott's (1970) and Calladine's (1988) analysis of the longitudinal curvature of the fold region in an isotropic tape spring.

For this particular tube hinge design, the paper presents three different analyses of the peak strains induced by the folding process. The geometric and material properties of the hinge are presented in the next section. The first analysis, presented in the section entitled "Analytical Estimates," obtains general analytical expressions for the longitudinal fold radius of a tape spring and the associated peak fiber stresses and strains. The second analysis is a finite-element simulation of the folding of a single tape spring and the third analysis is a finite-element simulation of a complete tube hinge. The predictions obtained from the three approaches are compared in the "Results" section, and a discussion concludes the paper.

Geometrical and Material Properties

The tube hinges considered in this paper are 82 mm long and have a circular cross section with radius $R=6.5$ mm. In the central section there are three 50-mm-long tape springs, each subtending an angle of 70°, thus leaving 50° for each slot. The slots are machined with end radii of 3 mm.

The tube hinges are made from plain weave carbon fiber T300/913 prepregs [plain weave, 913C-814-40% with a total fiber content of 60%, produced by Hexcel (Duxford, U.K)]. The properties of this prepreg are given in Table 1. Two particular layups will be considered for the tube hinges, a one-ply and a two-ply laminate with fibers at +45 and −45° to the axis of the tube hinge. The thicknesses of these laminates, based on measurements presented in Yee and Pellegrino (2005) are 0.27 and 0.47 mm, respectively. The geometric properties of the tube hinges are summarized in Table 2.

Table 1. Properties of 913C-814-40% Prepregs

Elastic moduli, $E_{11} \approx E_{22}$	46.0 (kN/mm^2)
Shear modulus, G_{12}	4.5 (kN/mm^2)
Poisson's ratio, $\nu_{12}=\nu_{21}$	0.065

Table 2. Geometry of Tube Hinges

Tape spring length, L		50 mm
Midsurface transverse radius, R		6.5 mm
Subtended angle, θ		70°
Thickness, t	laminate [±45]	0.27 mm
	laminate $[\pm 45]_2$	0.47 mm

The maximum bending strains that can be survived by (flat) laminates made from these prepregs were measured by Yee and Pellegrino (2005). The one-ply laminate, folded into a cylindrical surface whose axis is perpendicular to one set of fibers and parallel to the other set, fails when the maximum surface strain in the direction of the fibers is 2.7% (note that this value is larger than the failure strain in pure tension or compression), whereas the two-ply laminate fails at a strain of about 2.0%. On the other hand, when these laminates are folded into a cylindrical surface whose axis is at 45° to the fibers, they fail when the maximum bending strain is in excess of 5%, corresponding to a surface strain of 2.5% along the fibers.

Hence, taking in each case the lower fiber strain as the limiting value, it will be assumed that a one-ply hinge can survive surface strains along the fibers of up to 2.5%, whereas for a two-ply hinge a strain limit of 2.0% will be assumed. These values will be used to assess the feasibility of designing tube hinges with the properties given previously.

Analytical Estimates

Consider a tape spring of length L, uniform thickness t, and transverse radius of curvature R, whose cross section subtends an angle θ, as shown in Fig. 3(a). This section presents a simple analytical model for estimating the longitudinal radius of curvature, r, of the fold region—shown in Fig. 3(c)—for the case of composite tape springs made from 0,90 prepregs such as those

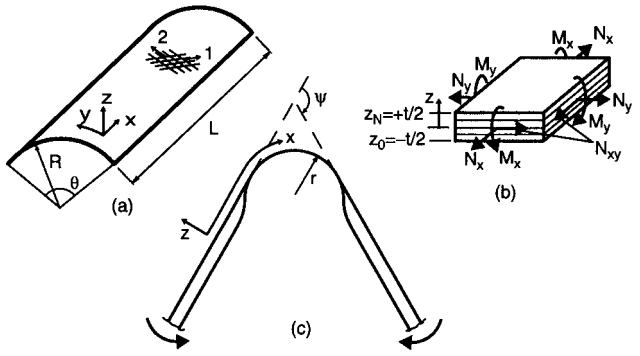

Fig. 3. (a) Initial configuration of tape spring; (b) definition of stress resultants (M_{xy} not shown); and (c) folded configuration

described in the section "Geometrical and Analytical Properties." The maximum strain in the fold region is also predicted.

It is assumed that the tape spring is made from a composite laminate, where lamina k—which is assumed to be in a state of plane stress—is orthotropic and has elastic stiffnesses Q_{ij}, i.e., (Jones 1999)

$$\begin{bmatrix} \sigma_1 \\ \sigma_2 \\ \tau_{12} \end{bmatrix} = \begin{bmatrix} Q_{11} & Q_{12} & 0 \\ Q_{12} & Q_{22} & 0 \\ 0 & 0 & Q_{66} \end{bmatrix} \begin{bmatrix} \epsilon_1 \\ \epsilon_2 \\ \gamma_{12} \end{bmatrix} \tag{1}$$

where the stress/strain axes 1 and 2 are aligned with the fiber directions.

A standard transformation of Eq. (1) to the global curvilinear coordinate system x,y,z shown in Fig. 3(a) gives

$$\begin{bmatrix} \sigma_x \\ \sigma_y \\ \tau_{xy} \end{bmatrix} = \begin{bmatrix} \bar{Q}_{11} & \bar{Q}_{12} & \bar{Q}_{16} \\ \bar{Q}_{12} & \bar{Q}_{22} & \bar{Q}_{26} \\ \bar{Q}_{16} & \bar{Q}_{26} & \bar{Q}_{66} \end{bmatrix} \begin{bmatrix} \epsilon_x \\ \epsilon_y \\ \gamma_{xy} \end{bmatrix} \tag{2}$$

The tape springs that are of specific interest for the present study have the 1,2 coordinate system at 45° to x,y, hence

$$\bar{Q}_{16} = \bar{Q}_{26} = 0 \tag{3}$$

Assuming that plane sections remain plane, the laminate stiffness matrix is obtained from classical lamination theory (Jones 1999)

$$\begin{bmatrix} N_x \\ N_y \\ N_{xy} \\ M_x \\ M_y \\ M_{xy} \end{bmatrix} = \begin{bmatrix} \mathbf{A} & \mathbf{B} \\ \mathbf{B} & \mathbf{D} \end{bmatrix} \begin{bmatrix} \epsilon_x^0 \\ \epsilon_{y0} \\ \gamma_{xy}^0 \\ \kappa_x \\ \kappa_y \\ \kappa_{xy} \end{bmatrix} \tag{4}$$

Eq. (4) is a relationship between the stress resultants per unit length—i.e., the normal and in-plane shear forces per unit length, N_x,N_y,N_{xy}, and bending and twisting moments per unit length, M_x,M_y,M_{xy}—with the corresponding deformation variables—i.e., the midplane strains, $\epsilon_x^0,\epsilon_y^0,\gamma_{xy}^0$, and the mid-plane curvatures, $\kappa_x,\kappa_y,\kappa_{xy}$. The sign convention for deformations is that they are positive in a sense such that the corresponding positive stress resultants do positive work.

If the prepregs are arranged symmetrically, as it is the case for the tube hinges that are being considered in this paper, we have a symmetric laminate and hence $\mathbf{B}=0$ (Jones 1999). Therefore, stretching and bending are decoupled and, since no stretching of the midsurface of the tape spring will be allowed, only the **D** matrix is of interest for the rest of the analysis.

In general (Jones 1999)

$$D_{ij} = \frac{1}{3}\sum_{k=1}^{n} (\bar{Q}_{ij})_k ((z_k)^3 - (z_{k-1})^3) \tag{5}$$

where n=number of laminas and $k=1$ is the bottom lamina. From Eqs. (3) and (5) $D_{16}=D_{26}=0$. Therefore

$$\begin{bmatrix} M_x \\ M_y \end{bmatrix} = \begin{bmatrix} D_{11} & D_{12} \\ D_{12} & D_{22} \end{bmatrix} \begin{bmatrix} \kappa_x \\ \kappa_y \end{bmatrix} \tag{6}$$

and the third relationship is simply $M_{xy}=D_{66}\kappa_{xy}$, which, however, will not be needed for the rest of the analysis, as x and y are axes of principal curvature in the fold region, i.e., $\kappa_{xy}=0$.

Radius of Curvature of Fold Region

Consider a tape spring in which a localized elastic fold has been formed, as shown in Fig. 3(c). Here ψ denotes the angle of the fold—i.e., the angle between the almost straight zones on either side of the fold—and r the longitudinal radius of curvature of the fold region. For isotropic tape springs Rimrott (1970) and Calladine (1988) have shown that $r=R$ by minimizing the total strain energy in the fold region with respect to r, for a given angle ψ. Their derivation assumes that the transition regions are unaffected by a change of r and hence need not be considered in the analysis; the same simplifying assumption will be made in the present analysis.

In the initial configuration the tape spring has principal curvatures $(0,+1/R)$ in the x and y directions, respectively, everywhere. In the deformed configuration these principal curvatures become $(+1/r,0)$ for equal sense bending and $(-1/r,0)$ for opposite-sense bending, in the fold region. Hence, the principal curvature changes in the fold region are

$$(\Delta\kappa_x,\Delta\kappa_y) = \left(\pm\frac{1}{r},-\frac{1}{R}\right) \tag{7}$$

where the positive and negative signs in the first term refer to equal and opposite sense bending, respectively.

The bending strain energy per unit area of shell is given by Mansfield (1989)

$$u = \frac{1}{2}\begin{bmatrix} \Delta\kappa_x & \Delta\kappa_y \end{bmatrix} \begin{bmatrix} M_x \\ M_y \end{bmatrix} \tag{8}$$

Substituting Eq. (6) and expanding

$$u = \tfrac{1}{2}(D_{11}\Delta\kappa_x^2 + 2D_{12}\Delta\kappa_x\Delta\kappa_y + D_{22}\Delta\kappa_y^2) \tag{9}$$

To obtain the total strain energy, the energy per unit area is multiplied by the area of the fold region, $Rr\psi\theta$. Then, substituting Eq. (7) and simplifying

$$U = \frac{R\theta\psi}{2}\left(\frac{D_{11}}{r} \mp \frac{2D_{12}}{R} + \frac{rD_{22}}{R^2}\right) \tag{10}$$

Minimizing U with respect to r

$$\frac{dU}{dr} = \frac{R\theta\psi}{2}\left(-\frac{D_{11}}{r^2} + \frac{D_{22}}{R^2}\right) = 0 \tag{11}$$

which gives

$$r = \sqrt{\frac{D_{11}}{D_{22}}}R \tag{12}$$

An expression identical to Eq. (12)—but considering only opposite-sense bending—was obtained by Schulgasser (1992). Note that for isotropic tape springs $D_{11}=D_{22}$ and hence $r=R$, as already known; also note that the radius of the fold is independent of the sense of bending.

Maximum Strains in Fold Region

Since the fold region is subject to pure bending and the laminate is symmetric, ϵ_x and ϵ_y are zero on the midplane. They vary linearly through the thickness and their maximum values are reached on the top and bottom surfaces of the tape spring

Table 3. Analytical Predictions of Maximum Strains (%) in One-Ply $[\pm 45^\circ]$ Tape Spring

Bending mode	Location	ϵ_x	ϵ_y	ϵ_f
Equal sense	$+t/2$	2.08	−2.08	0.0
	$-t/2$	−2.08	2.08	0.0
Opposite sense	$+t/2$	−2.08	−2.08	−2.08
	$-t/2$	2.08	2.08	2.08

$$\epsilon_x = \pm \frac{t}{2}\Delta\kappa_x, \quad \epsilon_y = \pm \frac{t}{2}\Delta\kappa_y \tag{13}$$

where the positive and negative signs correspond to $z=+t/2$ and $z=-t/2$, respectively. Substituting Eqs. (7) and (12) into Eq. (13) the maximum principal strains are found to be

$$\epsilon_x = \pm \sqrt{\frac{D_{22}}{D_{11}}}\frac{t}{2R} \tag{14}$$

where the sign is + for equal-sense bending and $z=+t/2$, or for opposite-sense and $z=-t/2$; whereas the sign is − for equal-sense bending and $z=-t/2$, or for opposite-sense and $z=+t/2$. And

$$\epsilon_y = \mp \frac{t}{2R} \tag{15}$$

where the sign is − at $z=+t/2$ and + at $z=-t/2$, regardless of the sense of bending. Since x and y are principal directions of curvature, $\gamma_{xy}=0$.

The corresponding stresses can be obtained from Eq. (2) which can be reduced to

$$\begin{bmatrix} \sigma_x \\ \sigma_y \end{bmatrix} = \begin{bmatrix} \bar{Q}_{11} & \bar{Q}_{12} \\ \bar{Q}_{12} & \bar{Q}_{22} \end{bmatrix} \begin{bmatrix} \epsilon_x \\ \epsilon_y \end{bmatrix} \tag{16}$$

Application to One-Ply Tape Spring

A 0.27-mm thick one-ply tape spring with fibers at +45° and −45° is considered. The lamina stiffness matrix, Q_{ij}, the transformed lamina stiffness matrix, $\bar{Q}_{ij}$, and the relevant part of the laminate stiffness matrix can be readily calculated from the experimental data presented in Table 1, using *VISILAM* (Avery 1998)

$$\bar{Q}_{11} = \bar{Q}_{22} = 29.1 \times 10^3 \text{ N/mm}^2$$

$$\bar{Q}_{12} = 20.1 \times 10^3 \text{ N/mm}^2$$

and

$$D_{11} = D_{22} = 47.7 \text{ N mm}$$

$$D_{12} = 33.0 \text{ N mm}$$

Since $D_{11}=D_{22}$, Eq. (12) gives

$$r = R = 6.5 \text{ mm} \tag{17}$$

and hence this tape spring behaves like an isotropic one.

The maximum principal strains on the top and bottom surfaces of the tape spring can then be obtained from Eqs. (14) and (15), and are presented in Table 3. It is particularly useful to compute the strain along the fibers, ϵ_f, by means of a strain transformation, as its value can then be compared to the failure strain in bending of a single-ply lamina, quoted in the section entitled "Geometrical and Material Properties." The value of ϵ_f in the direction +45° is presented in the last column of Table 3. The maximum strains in a two-ply $[\pm 45^\circ]_2$ tape spring can be calculated in a similar way.

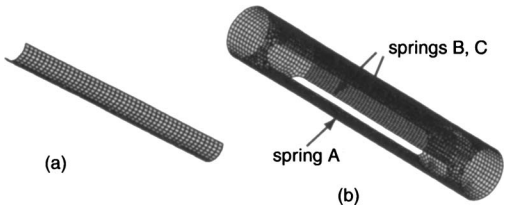

Fig. 4. Typical finite element models of (a) tape spring and (b) tube hinge

Simulation of Folding Process

Detailed simulations of the folding of a single tape spring and of a complete tube hinge, consisting of three identical tape springs, were carried out with the *ABAQUS* (2003) finite element package. Both one-ply and two-ply tape springs were analyzed, and the linear-elastic material properties presented in Table 1 were assumed.

One reason for carrying out these simulations is to assess the accuracy of the simple analytical model presented in the previous section, and to identify any limitations. Also, by comparing the deformation of a single tape spring with that of a tape spring that is part of a tube hinge, one can better understand the behavior of tube hinges, and thus obtain simple estimates of the maximum strains caused by folding.

Finite Element Model

Since the interaction between the bending and stretching stiffnesses of the tape springs that make up a tube hinge plays an important role in determining its overall structural behavior, thin shell elements are clearly the most appropriate choice. *ABAQUS* Standard (2003) offers several shell elements, and preliminary runs were carried out with four-node quadrilateral full integration general purpose elements (S4); these elements have six degrees of freedom at each node. Four-node reduced integration shell elements (S4R5) with five degrees of freedom per node were also investigated. Eventually, the latter element was adopted, as it performs well for large rotations with only small strains, uses reduced integration with hourglass control to prevent shear locking, and is computationally economical.

A typical mesh for a tape spring involved 200 elements lengthwise by 30 elements widthwise. The mesh for a complete tape tube hinge had a similar mesh density, and hence the number of elements was proportionally larger, see Fig. 4.

Simulation Techniques

The multiple point constraint (MPC) option was used to define the boundary conditions. For both the tape spring and the tube hinge models, the nodes on either end were tied to a MPC node, located at the centroid of the end cross section, through rigid beam elements. The main reason for locating the MPC nodes at the centroid is that at the beginning of the loading process the structure will thus be under pure bending when rotations are applied at the ends.

The three tape springs that constitute a tube hinge come into

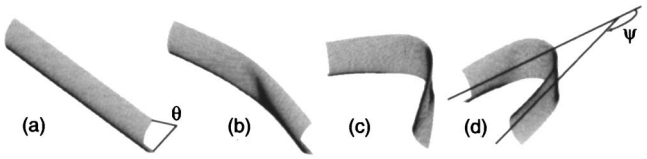

Fig. 5. Folding sequence of tape spring subject to opposite-sense bending: (a) $\psi=0°$; (b) $\psi=30°$; (c) $\psi=113°$; and (d) $\psi=170°$

contact during the folding process; hence contact between these tape springs needs to be suitably modeled. ABAQUS defines the contact conditions between two bodies using a strict "master-slave" algorithm. The (*CONTACT PAIR) option needs to be specified for the two deformable surfaces, one of which is defined as the master surface and the other as the slave surface. In addition, the INTERACTION parameter is used to associate the contact pairs being defined with a surface interaction model, such as friction. The SMALL SLIDING parameter was chosen, instead of the standard FINITE SLIDING, to achieve greater sensitivity to local initial gaps at the interface, caused by mismatch in the discretization of meshed surfaces that come into contact. The SLIDING parameter sets up a slave node that interacts with the same region of the master surface throughout the analysis, despite the large displacements that occur during the simulation. The SURFACE BEHAVIOR parameter was set to the default, PRESSURE-OVERCLOSURE=HARD; this option provides arbitrarily large contact forces as soon as the surfaces come into contact.

After having unsuccessfully attempted to use the default contact definition, a *symmetric* master-slave approach was adopted, i.e., two sets of contact pairs were defined for the same two surfaces, switching the roles of master and slave between the two surfaces. Despite involving additional computations, this approach was found to provide improved convergence and greater accuracy.

A geometrically nonlinear (*NLGEOM) incremental analysis was carried out using the Newton–Raphson solution method, with automatic stabilization provided through the STABILIZE function. This solution option automatically introduces pseudoinertia and pseudoviscous forces at all nodes when an instability is detected. Instead of continuing with the standard quasi-static analysis, Abaqus automatically switches to a pseudodynamic integration of the equations of motion for the structure, thus avoiding numerical singularities. The pseudoviscous forces are calculated based on the model's response in the first increment of the analysis step, by assuming that the dissipated energy is a fraction of the strain energy during the first step. This fraction is known as *damping intensity*, and has a default value of 2×10^{-4}. To attain accurate results, it is desirable to set this parameter to the lowest value at which convergence is achieved. In most of the analyses presented in the next section the damping intensity was set to 1×10^{-8}.

Results

This section presents the finite element simulation results for both the tape spring and the tube hinge, and compares the maximum strains and fold radii obtained from these detailed analyses with results from the simple analytical model presented in the section entitled "Analytical Estimates."

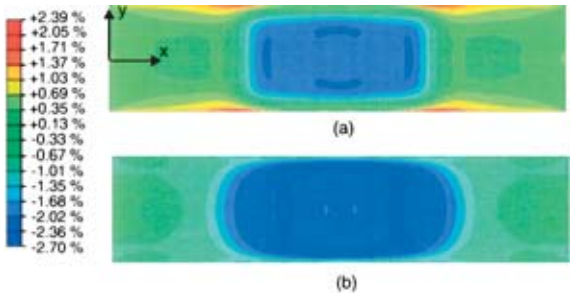

Fig. 6. (Color) Principal strains on surface $z=+t/2$ of one-ply tape spring under opposite-sense bending: (a) maximum principal strain, ϵ_x; and (b) minimum principal strain, ϵ_y

Folding of Tape Spring

Fig. 5 shows a series of snapshots from the folding sequence of a one-ply $[\pm45°]$ tape spring subject to opposite-sense bending, under monotonically increasing end rotations of the two MPC nodes. The tape spring has a cross-sectional radius $R=6.5$ mm and subtends an angle $\theta=130°$.

The FE simulation provides the entire strain field in the folded tape spring, from which a key assumption of the analytical model, namely that both the longitudinal and transverse curvatures are uniform throughout the fold region, can be verified.

Figs. 6 and 7 show contour plots of the principal strains for opposite-sense and equal-sense bending of the tape spring, respectively. Only the strains on the surface $z=+t/2$ are shown, as the distribution on the opposite surface is practically identical, but with the sign reversed, thus indicating that the shell is in pure bending throughout. This observation confirms the validity of a key assumption made in setting up the analytical model, namely that the mid-plane normal strains are negligibly small. Note that the strain distribution is uniform through the central part of the tape spring, corresponding to the fold region, hence confirming that this region is uniformly curved. Also note that under opposite-sense bending—which causes high biaxial compressive strains in the fold region—high tensile strains occur in four corner regions that are symmetrically located with respect to the fold, see Fig. 6(a).

Of particular importance to the design of a composite tape spring is the peak strain along the fibers, ϵ_f, which has been plotted in Fig. 8 for the particular fibers at +45° to the axis of the tape spring. The first thing to note in Fig. 8 is that the largest strain, of around −2.3%, occurs when the tape spring is subject to opposite-sense bending; this result agrees with the analytical pre-

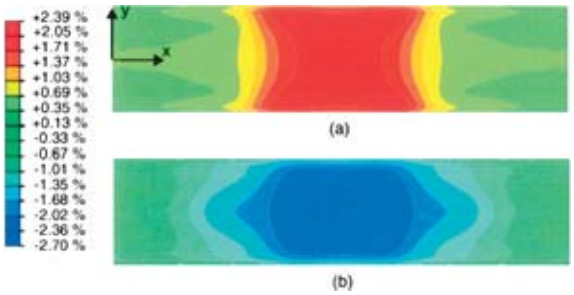

Fig. 7. (Color) Principal strains on surface $z=+t/2$ of one-ply tape spring under equal-sense bending: (a) maximum principal strain, ϵ_x; and (b) minimum principal strain, ϵ_y

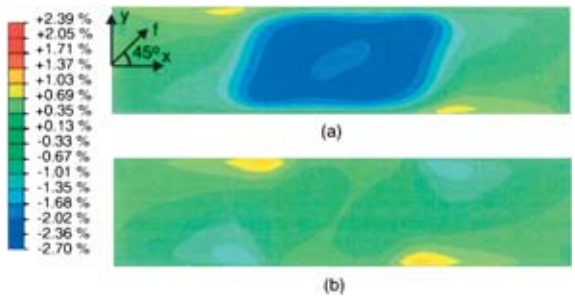

Fig. 8. (Color) Strain along fibers at +45°, on surface $z=+t/2$ of one-ply tape spring for (a) opposite-sense bending and (b) equal-sense bending

Table 4. Fold Radii and Maximum Strains in Tape Springs from ABAQUS

Laminate	Bending mode	θ (deg)	r (mm)	ϵ_f (%)
One-ply	Opposite sense	70	9.27	−1.91, 1.77
[±45°]		90	8.11	−2.01, 1.97
		110	7.35	−2.17, 2.10
		120	6.96	−2.27, 2.17
		130	6.52	−2.37, 2.25
	Equal sense	130	6.57	−1.26, 1.02
Two-ply	Opposite sense	130	7.16	−3.78, 3.61
$[\pm 45°]_2$		140	6.65	−3.93, 3.73
		150	6.49	−4.10, 3.88
	Equal sense	150	6.53	−2.06, 1.68

dictions in Table 3. In the case of opposite-sense bending, Fig. 8(a), fairly large tensile strains occur in two small regions on either side of the fold. There are only two such regions, not four as in the case of principal strains, because here we are considering the strain along one particular set of fibers. In the case of equal-sense bending, Fig. 8(b), the strain in the central part of the fold region is quite small—again, as expected from Table 3—and so the largest strains occur in the small regions on either side of the fold. These peak localized strains, of up to −1.3%, are much smaller in magnitude than the maximum fiber strains for the case of opposite-sense bending, which are −2.4%.

The characteristic tape-spring behavior that has been seen throughout this paper, where the deformation is concentrated in a uniformly curved fold region—as opposed to the uniform deformation that would be observed in a *flat strip* subject to the same end rotations—requires that the angle θ subtended by the cross section be sufficiently large to trigger this type of behavior. How large this angle needs to be depends on the interaction between out-of-plane bending and in-plane stretching, as well as on the degree of anisotropy of the tape spring.

In the absence of a general, analytical expression for this limiting value of θ, a parametric study was carried out into the effect of gradually increasing θ in one-ply [±45°] and two-ply $[\pm 45°]_2$ tape springs. The study focused on tape springs under opposite-sense bending but, once the critical value of θ had been identified, it was checked that the same value of θ would give the same type of behavior also for equal-sense bending. In all cases, a total rotation $\psi=170°$ of one end of the tape spring, with respect to the other end, was imposed.

The results of this study, in terms of the variation of the radius of longitudinal curvature at the center of the tape spring, and the peak tensile and compressive strains are presented in Table 4. Because θ does not appear in Eq. (12), the analytical prediction for r is 6.50 mm in all cases.

For the smaller θ's the longitudinal radius of the fold region, r, of the one-ply tape spring is about 50% larger than the transverse radius of the undeformed cross section, $R=6.5$ mm. The maximum strains are inversely proportional to the curvature, and hence much smaller. For reference, note that a 50 mm long, flat strip subject to a total rotation $\psi=170°$ (=2.97 rad) would have $r=50/2.97=16.8$ mm. Hence, clearly some localization of the deformation has already been achieved for $\theta=70°$, although the fold radius continues to become tighter until $\theta=130°$ in the one-ply tape spring and $\theta=150°$ in the two-ply one.

Folding of the Tube Hinge

Fig. 9 shows four configurations of a one-ply tube hinge. In Fig. 9(a) the tube hinge is undeformed, hence $\psi=0$. In Fig. 9(b), corresponding to a rotation $\psi\approx 43°$ between the two ends, a localized fold has formed in Spring A, which is under opposite-sense bending. Springs B and C are under equal-sense bending plus some twisting. Two localized folds have formed in each spring, but so far have joined up only on one edge. The first contact between Spring A and Springs B and C occurs at $\psi\approx 79°$; they remain in contact from then on. Fig. 9(c), corresponding to $\psi\approx 82°$, shows a single localized fold in each tape spring, with the fold in Spring A providing an outer constraint for the folds in Springs B and C. In Fig. 9(d), corresponding to a rotation $\psi\approx 170°$, the end tubes also come into contact. This interference can be avoided by adding two small, equal and opposite shear forces at the ends of the tube hinge, in addition to the pure moments which have driven the folding process.

Fig. 10 shows contour plots of the surface strains along the fibers at +45°. It is interesting to note that the strain distribution in the outer surface of Spring A, Fig. 10(a), is similar to that on the surface $z=+t/2$ of a tape spring on its own, Fig. 8(a). Also, the strain distribution on the inner surface of Spring A, Fig. 10(b), is essentially equal and opposite to that on the outer surface. This indicates that, as already for the case of a tape spring on its own, the midplane strains are again negligibly small.

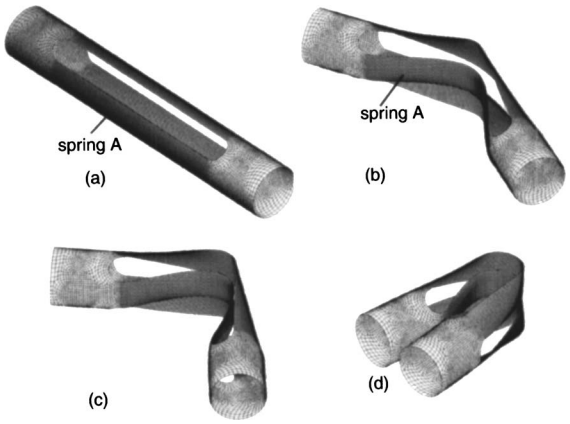

Fig. 9. Folding sequence of tube hinge: (a) $\psi=0°$; (b) $\psi\approx 43°$; (c) $\psi\approx 82°$; and (d) $\psi\approx 170°$

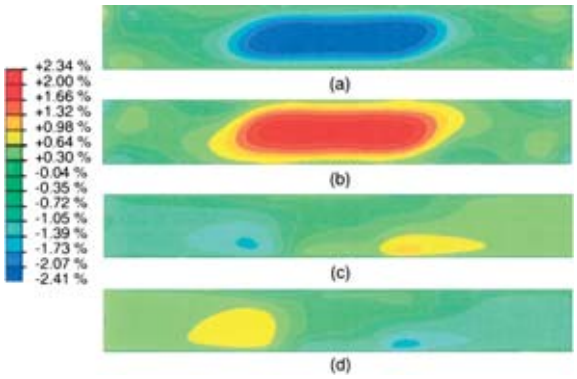

Fig. 10. (Color) Strain along fibers at +45° for one-ply tube hinge. Spring A, (a) outer surface and (b) inner surface; Spring B, (c) outer surface and (d) inner surface

Figs. 10(c and d) show contour plots of the surface strains on Spring B; note that they are generally much smaller than in Spring A; the peak values are about half of those in Spring A. It is interesting to note that, because Spring B has been twisted as well as bent, the regions of high localized fiber strain magnitudes in Figs. 10(c and d) are both on the same edge of the tape spring, whereas in Fig. 8(b) they are on either edge.

The moment–rotation plot obtained from this simulation is shown in Fig. 11. Note that the hinge behaves approximately linearly for rotations $\psi < 7.7°$; at $\psi = 7.7°$ a limit point is reached and the corresponding moment is 940 N mm. The tube hinge then gradually softens, reaching a minimum moment of ≈236 N mm which remains practically constant over a large range of ψ. The response upon unloading has not been investigated.

If the direction of ψ is reversed the hinge response is again initially approximately linear, but this time Springs B and C are under opposite-sense bending and so the limit moment is higher, −1,363 N mm, at a rotation $\psi = 1.5°$. As for positive moments, the tube hinge then softens, reaching a minimum moment amplitude of −362 N mm at $\psi = -42.2°$.

A comparison of the fiber strains predicted by the simple analytical model with the finite-element predictions, using both the single tape-spring model (recall that here the angle subtended is $\theta = 130°$) and the complete hinge model (here each tape subtends an angle $\theta = 70°$), is presented in Table 5. Note that the analytical predictions for the largest fiber strain—which occur in the tape

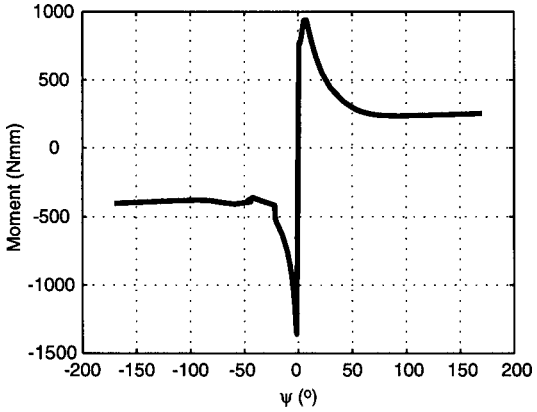

Fig. 11. Moment–rotation finite-element relationship for one-ply tube hinge

Table 5. Maximum Strains (%) along Fibers in Tube Hinges

					ABAQUS	
Laminate	Spring	Bending mode	Location	Analytical	Tape spring	Tube hinge
One-ply [±45°]	A	Opposite sense	Outer	−2.08	−2.37	−2.41
			Inner	2.08	2.25	2.34
	B, C	Equal sense	Outer	0.00	−1.26, 1.23	−1.20, 1.20
			Inner	0.00	1.02, −1.33	−1.27, 1.04
Two-ply $[±45°]_2$	A	Opposite sense	Outer	−3.62	−4.10	−3.72
			Inner	3.62	3.88	3.31
	B, C	Equal sense	Outer	0.00	−2.06, 1.90	−1.58, 1.48
			Inner	0.00	−2.02, 1.68	−1.61, 1.48

spring under opposite-sense bending—are underestimated by 10–15% when compared with the most accurate estimate, i.e., the complete hinge model. The analytical predictions for the maximum fiber strain in Springs B and C, which are under equal-sense bending, are not accurate—for the reasons already discussed in the section entitled "Folding of Tape Spring." However, note that in these springs the peak strains are about half of those in Spring A.

Discussion and Conclusions

The first part of this paper has presented an extension to orthotropic shells of Rimrott's (1970) and Calladine's (1988) analytical model for predicting the longitudinal fold radius, r, of the uniformly curved region at the center of an isotropic, tape spring with transverse radius of curvature R. It has been shown that

$$r = \sqrt{\frac{D_{11}}{D_{22}}} R \tag{18}$$

for both equal- and opposite-sense bending of the tape spring. The corresponding principal strains and stresses in this curved region, which are in the longitudinal and transverse directions, can be estimated from Eqs. (14)–(16). From these, the peak fiber strains can be obtained from a standard strain transformation.

Next, a detailed study of the deformation and strains induced by folding CFRP tape springs and tube hinges with a ±45° lay-up has been presented. This study has shown that the largest fiber strains in tape springs under opposite-sense bending occur in the uniformly curved fold region and can be predicted analytically with good accuracy. The same approach also gives accurate predictions for the *maximum principal strains* in tape springs under equal-sense bending, which also occur in the uniformly curved fold region. However, in this case the *maximum fiber strains* occur in small regions at the edge of the fold, and for two specific cases that have been analyzed in detail it has been found that these maximum fiber strains are around 50% of the maximum principal strain in the fold region.

It thus follows that the design of composite tape springs is significantly different from that of metallic tape springs, mainly because yielding in metals takes place under high shear. A metallic tape spring is closest to yielding when it is under equal-sense bending; in this case the maximum shear stress, τ_{max}, is approximately equal in magnitude to the longitudinal and transverse stresses (which have opposite signs). On the other hand, when a metallic tape spring is under opposite-sense bending, $\tau_{max} \approx 0$ in the fold region, as the two principal stresses are approximately

equal. All of this is opposite to a composite tape spring with fibers at +45 and −45°, which fails when the fiber strain is too high.

A parametric study of the effects of varying the angle θ subtended by the cross section has been conducted, showing that the longitudinal radius of curvature at the center of a folded one-ply $[\pm 45^\circ]$ tape spring decreases by about 30% when θ is increased from 70 to 130°. Thus, a tape spring with $\theta \approx 130^\circ$ fully shows the characteristic, localized fold that is observed in steel tape measures, both for opposite-sense and equal-sense bending. The two-ply $[\pm 45^\circ]_2$ tape spring also converges to the analytically estimated value of r, but an even larger subtended angle, $\theta = 150^\circ$, is required. Clearly, the increased bending stiffness of the thicker laminate requires a larger subtended angle for the stretching-dominated behavior to take over.

From a design viewpoint, the principal attraction of tape springs with larger θ's is that they snap firmly into the straight configuration—a very attractive feature in the design of self-latching hinges—and form well-identified folds with radius of curvature insensitive to the fold angle. However, smaller θ's will generally result in smaller strains.

Finally, an 82 mm long tube hinge with a diameter of 13 mm, consisting of three tape springs has been investigated. It has been found that contact between the tape springs occurs at fold angles of around 80°, but does not affect substantially the distribution and magnitude of the maximum fiber strains. A finite-element analysis of a single tape spring with identical properties to the tape springs that make up the tube hinge provided, for both cases that have been considered, conservative estimates of the peak strains. These estimates were particularly accurate for the single-ply tube hinge.

It has been shown (in Table 5) that an 82-mm-long tube hinge with a cross-sectional radius of 6.5 mm and 50-mm-long tape springs would be subject to a maximum fiber strain of −2.4% in the folded configuration, if made from a one-ply, 0.27-mm-thick 913C-814-40% prepreg with fibers at +45 and −45° to the longitudinal axis. This strain is just within the limit of the material. A tube hinge made from a two-ply laminate, would be 0.47 mm thick and would be subject to maximum strains well in excess of the material limit. For this laminate to survive the folding process, the cross-sectional radius of the tube should be increased, or at least the radius of the tape spring that goes into opposite-sense bending.

In concluding, it is noted that the limiting strains measured by Yee and Pellegrino (2005) were obtained from uniaxial bending tests. Biaxial bending test data are currently unavailable.

Acknowledgments

The writers are grateful to Dr M. F. Sutcliffe of Cambridge University for help and advice, and to Professor C. R. Calladine for comments on an earlier version of this paper. Mr. G. C. Dando and Dr. A. Freeman, of QinetiQ Ltd., have provided sample tube hinges and have offered advice on many occasions. Mr. J. Ellis, of Hexcel, Duxford, U.K., has provided materials and manufacturing facilities. Financial support from Corpus Christi College, Cambridge, and QinetiQ Ltd. is gratefully acknowledged.

Notation

The following symbols are used in this paper:

D = bending stiffness;
L = length of tape spring;
M = bending or twisting moment per unit length;
N = normal or in-plane shear force per unit length;
n = number of laminas;
$Q_{ij}, \bar{Q}ij$ = lamina stiffnesses;
R = initial transverse radius of curvature;
r = longitudinal radius of curvature of fold region;
t = thickness;
U = total strain energy;
u = strain energy per unit area;
γ = shear strain;
Δ = change;
ϵ = normal strain;
κ = bending or twisting curvature;
σ = normal stress;
τ = shear stress.
θ = angle subtended by cross section; and
ψ = fold angle.

Subscripts

k = lamina index;
x,y,z = longitudinal, transverse, and normal directions; and
1,2 = fiber directions.

References

Abaqus, Inc. (2003). *ABAQUS theory and standard user's manual, Version 6.2*, Pawtucket, R.I.

Avery, W. B. (1998). *VISILAM 4*, Boeing.

Calladine, C. R. (1988). "Love Centenary Lecture: The theory of thin shell structures 1888–1988." *Proc. Inst. Mech. Eng.*, 202(42), 1–9.

Jones, R. M. (1999). *Mechanics of composite materials*, 2nd Ed., Taylor & Francis, Philadelphia.

Mansfield, E. H. (1989). *The bending and stretching of plates*, 2nd Ed., Cambridge University Press, Cambridge, U.K.

Rimrott, F. P. J. (1970). "Querschnittsverformung bei Torsion offener profile." *ZAMM*, 50, 775–778.

Schulgasser, K. (1992). "Configuration of a bent tape of curved cross-section." *Trans. ASME J. Appl. Mechanics*, 59(September), 692–693.

Seffen K. A., and Pellegrino, S. (1999). "Deployment dynamics of tape springs." *Proc. R. Soc. London, Ser. A*, 455, 1003–1048.

Yee, J. C. H. and Pellegrino, S. (2005). "Folding of woven composite structures." *Composites, Part A*, 36(2), 273–278.